4.1 Final publishable summary report

4.1.1 Executive Summary

Four different thermal management concepts were investigated in order to improve the thermal protection capabilities for future reusable space vehicles during atmospheric entry and for hypersonic transport vehicles during flight. In a first step, the requirements for thermal management were compiled for future missions. Based on the assessments a wing leading edge was defined as the baseline configuration for THOR. Specific reference configurations were defined which implement the key elements of the considered thermal management concepts into a leading edge geometry. For the considered thermal management concepts the physical potential for improvement was checked a priori based on existing measured data or simulations using appropriate models. In the conceptual of the project, the configurations were refined with particular focus to experimental concept verification in high enthalpy facilities. Convenient test configurations were identified for the arc-heated facility L3K and the shock tunnel HIEST.

In preparation of experimental verification, manufacturing of the ceramic materials and structures as well as their integration into the test assemblies were associated with several challenges. New processing routes were found for the production of large CMC parts with integrated highly conductive fibres. A newly developed replica technique starting from 3D-printed polymeric templates was developed for the preparation of SiC-based ceramic lattices. Appropriate joining techniques were established for the bonding between lattice and solid CMC. Structures for transpiration cooling were transferred to smaller scale by a new integration technique for porous materials based on electroplating. Manufacturing tasks were accompanied and supported by material characterization activities, which primarily focussed on the newly developed materials and high temperature joining techniques.

Leading edge test assemblies were prepared for experimental verification in L3K. The tests were carried out as transient tests to steady-state conditions. Temperature measurements were used to assess the thermal performance with particular consideration of thermal equilibration and reduction of the stagnation temperature. Thermal equilibration was observed mainly for the two passive cooling concepts. In particular, the opening of a small cavity at the nose with concept 1b resulted in a significant settlement of temperatures differences. Comparable temperature reductions were evaluated for the two passive concepts and the active concept 2a, all between 70 K and 80 K. By combining the two passive concepts, the temperature reduction could be enhanced to more than 100 K, allowing the material to sustain an additional heat load of more than 20% of the reference load. These results were verified by numerical rebuilding using coupled simulations.

For transpiration cooling, the interference of the emanating gas with the boundary layer, was investigated in the test campaign in the HIEST shock tunnel. At low Reynolds number conditions effective cooling was verified, but with increasing coolant flow rate the risk of boundary layer transition was found enhanced. This result was confirmed by numerical rebuilding as well.

Eventually, improvements to thermal management capabilities were verified for all four considered concepts. Experimental verifications tests indicated considerable reductions of stagnation temperatures the leading edge test configurations. These reductions are correlated with a potential to increase the applicable heat loads considerably. The experimental results confirm a TRL level of 2-3 for each concept. In addition, the investigations indicated potential for technical and methodical optimization. Accordingly, the evaluated improvements might be increased further.

4.1.2 Project Context and Objectives

Space vehicles are exposed to extreme thermal loads when entering a planetary atmosphere. To protect the vehicle's interior a thermal protection system (TPS) is required for both, manned missions and unmanned missions. The thermal management concept of state-of-the-art re-usable vehicles, as e.g. the Space Shuttle orbiter, is mainly based on an indirect strategy making use of the fact that heat loads can be controlled by choosing an appropriate external shape for the vehicle and an adequate entry trajectory. A sophisticated technical thermal management is not established, thermal balances are applied only locally providing information about required insulation thicknesses corresponding to the local heat flux. As a consequence, highly loaded vehicle components, as e.g. the nose and the leading edges of the wings, have a blunt shape. Aerodynamically, however, the bluntness is a major drawback, because it significantly reduces the vehicle's flight performance resulting in a very poor capability for fast corrections to the flight path by flying manoeuvres.

For future space vehicles significant improvements are required in the long term in flight performance. Next generation orbiters and to a huge extent hypersonic transport vehicles will need fast flight path control for efficient operation, a requirement that cannot be met with extremely blunted components. A significant reduction of bluntness, however, means significantly higher heat loads which are beyond the capabilities of the conventional thermal management concept. Thermal management concepts will need to be defined globally with a technically sophisticated implementation in order to meet the requirements. The main challenges for thermal management are

- equilibration of thermal loading by transferring heat efficiently from highly loaded surface areas to less loaded regions, and
- consideration and inclusion of active cooling techniques.

The SpaceLiner shown in Figure 1 is an example for an orbital transport vehicle for intercontinental passenger transport. It is based on rocket propulsion and had been introduced in 2005 as a conceptual study which is still going on. The flight scenario is correlated with extreme heat loads during atmospheric entry at nose and wing leading edges which are exceeding the capabilities and specifications of conventional reusable TPS systems by far. Correspondingly, a demand for new approaches in thermal protection including active cooling has been defined essential for the vehicle.

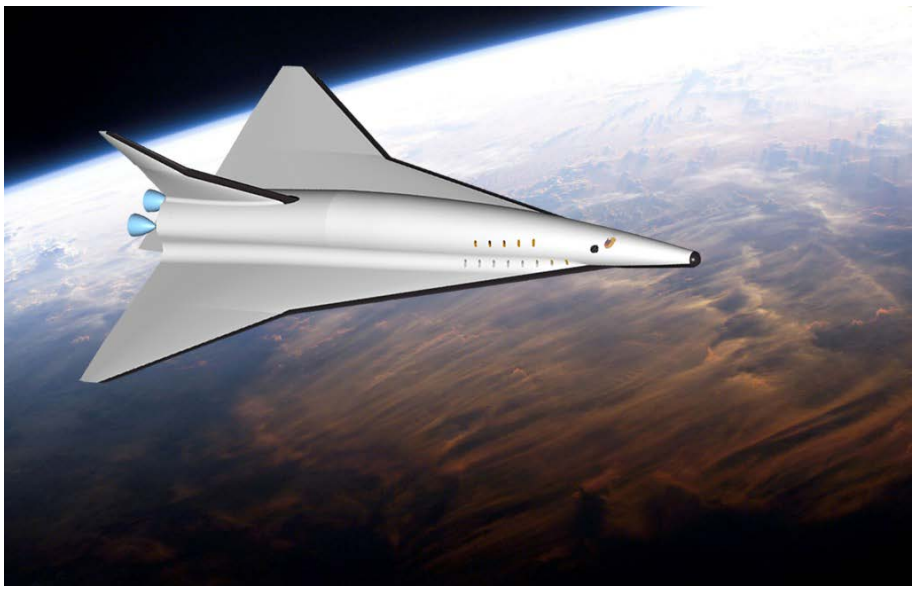

Figure 1: SpaceLiner for suborbital intercontinental travel

For starting development and validation of novel thermal management concepts the general conditions were promising due to recent progress in base material development. New materials with tailored properties were available for being integrated in thermal protection systems, as e.g.

- carbon-based fibres with a huge thermal conductivity which exceeds the conductivity of conventional fibres by at least an order of magnitude,
- SiC-based ceramic foams or lattices with operational temperatures being very close to those of conventional dense ceramic matrix composite (CMC) materials.

The THOR project thematically focussed on the development of new thermal management concepts which are specifically targeted to atmospheric entries of future space vehicles and hypersonic transport vehicles. The considered concepts are innovative solutions which are technologically based on recent improvements to materials and structures. The technical implementation included manufacturing aspects as well as a detailed physical modelling.

There are two principal options for dealing with the severe thermal environments encountered during atmospheric entry, i.e.

(1) passive cooling technologies, and
(2) active cooling technologies.

Both options were considered in THOR and two separate thermal management concepts were elaborated in detail for each option. Common and novel to all considered concepts was a globalized approach for thermal balancing and thermal management in order to improve the thermal capabilities of TPS systems and to increase the maximal tolerable heat loads.

Efficient thermal equilibration was the key element within the thermal management concepts based on passive cooling technologies aiming at an effective load balance by transfering heat from highly loaded areas to regions with a lower thermal loading. By utilizing different physical mechanisms for thermal equilibration, i.e. conductive heat transfer and radiative heat transfer, two concepts appeared promising:

(1a) Innovative composite materials with integrated highly conducting fibres,
(1b) TPS structures with intensive radiative heat exchange.

In concept 1a lateral heat conduction was promoted by introducing highly conductive fibres into a TPS skin material which should improve the capabilities for thermal equilibration significantly. Conventionally, fibres with a conductivity of 10 to 20 W/mK are being used. There are, however, pitch-based carbon fibres with a reported thermal conductivity of up to 1000 W/mK. An increase of the fibres' conductivity by at least one order of magnitude was expected realistic

Concept 1b is approaching thermal equilibration by heat exchange below the TPS skin. Advantage is taken from the long-distance thermal exchange capabilities of thermal radiation. According to the Stefan-Boltzmann relation, radiated heat strongly intensifies with temperature and therefore intrinsically supports thermal equilibration on a non-uniformly loaded curved structure.

Thermal management concepts for actively cooled components basically need a globalized consideration, since coolant supply and return are essential elements of the system. The two active cooling concepts which were considered in THOR use innovative structures with porous materials as passages for coolants. The concepts are called

(2a) Sandwich-TPS with ceramic foams,
(2b) Transpiration cooling of external surfaces.

In concept (2a) a novel sandwich structure should be developed which is made of two ceramic skin layers and a SiC-based ceramic foam or lattice in between. The foam/lattice is highly porous and therefore well-suited to pass the coolant along the back side of the external skin to highly loaded regions where it takes over the heat convectively, additionally reducing the surface temperature, taking advantage of the increased surface for heat exchange and of the high thermal conductivity of the ceramic struts as well.

For transpiration cooling in concept 2b, the coolants are supposed to be fed through porous surface elements to the exterior. In this case, cooling is achieved not only for the porous element itself, but also for regions downstream of transpired surface parts.

An additional concept was being considered as a reference for the evaluation of improvements with regard to thermal performance, i.e. concept

(0) Conventional CMC, fully insulated.

The technical considerations for each thermal management concept included

- detailed elaboration of the thermal management approach,
- technical implementation including sample manufacturing, and
- redundant consolidation of the concept by verification experiments and numerical simulation.

The main objective of the project was to design, develop, implement, test and validate the considered thermal management concepts for application to atmospheric entry of space vehicles and hypersonic transport. From this premise the following technical and non-technical objectives were defined:

- Definition and elaboration of the thermal management concepts;
- Development and manufacturing of all required ceramic matrix composite (CMC) materials;
- Elaboration of appropriate joining techniques for sandwich structures made of CMC skin materials and ceramic foams;
- Characterization of the mechanical and thermal properties for all newly developed materials and structures;
- Development of appropriate physical models for numerical consolidation;
- Design and manufacturing of validation samples for the experimental verification of the thermal management concepts;
- Experimental verification of the thermal management concepts in high enthalpy ground test facilities with
  - long-duration tests in arc-heated facilities at realistic heat loads and surface temperatures
  - short-duration test in a shock-tunnel facility at realistic flight conditions;
- Consolidation of the verification tests by coupled numerical simulations including fluid/structure interaction;
- Achievement of a TRL 2-3 of the new concepts at the end of the project;
- Synthesis of the achieved results with particular consideration of the requirements for future space missions;
- Elaboration of a use plan that identifies the necessities for technology transfer to space end users and evaluates potential spin-off applications;
- Dissemination of the technical progress using the most relevant communication channels.

4.1.3 Main S&T Results/Foregrounds

General Framework

The general framework for the project work was initially defined with a compilation of the requirements on thermal management of future reusable space vehicles and hypersonic transport vehicles. Based on the trade-off of several missions (see Figure 2) it was concluded that a wing leading edge was best-suited as a baseline configuration for the investigations in THOR, to satisfy the requirements for future vehicles. The main characteristics of the heat flux distribution on highly loaded vehicle components, i.e. high stagnation point heat fluxes which reduce towards adjacent areas considerably, can be reproduced on a leading edge geometry, while keeping geometric complexity for verification low, i.e. on two-dimensional level.

Figure 2: Considered configurations for atmospheric entry and hypersonic transport

First reference configurations were defined which implement the key elements of the considered thermal management concepts (as listed in Table 1) into a generic leading edge geometry. The reference configurations were then elaborated in more detail with particular focus to the preparation of experimental verification in high enthalpy facilities [1].

In parallel, the physical potential for improvement was checked a priori for each thermal management concept. For concepts 1b, 2a and 2b the proof could be accomplished based on available measured data from other projects. The check of concept 1a was based on new model considerations on the effective thermal conductivity of a CMC material with integrated highly conductive fibres [2]. In conventional SiC-based CMC materials, fibres with a conductivity of 10 to 20 W/mK are being used. There are, however, pitch-based carbon fibres with a reported thermal conductivity of up to 1000 W/mK. Accordingly; an increase of the fibres' conductivity by at least one order of magnitude was expected realistic.

Table 1: Considered Thermal Management Concepts

Type of cooling	Concept index	Concept name
passive	1a	Innovative composite materials with integrated highly conducting fibres
passive	1b	TPS structures with intensive radiative heat exchange
active	2a	Sandwich-TPS with ceramic foams
active	2b	Sandwich-TPS with ceramic foams
passive	0	Conventional CMC, fully insulated (reference)

The influence of the fibers' conductivity on the effective thermal conductivity of the composite material is shown in Figure 3. The results were obtained with two models, a block circuit (BC) and a finite element (FE) model, under the assumption that the fibers' conductivity does not change at elevated temperatures. In particular, for the in-plane conductivity a substantially higher conductivity is predicted when using highly conductive fibers.

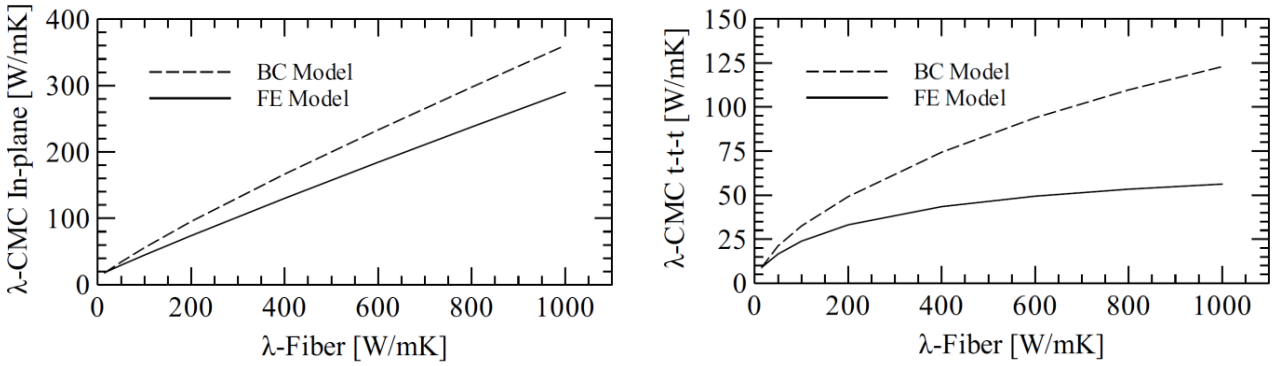

(a) parallel (in-plane) to fiber layers (b) perpendicular (out-of-plane) to fiber layers

Figure 3: Effective thermal conductivities of fiber-based CMC

Test Configurations

For experimental verification of the concepts two generic leading edge geometries were defined for thermal tests in DLR's arc heated facility L3K [3]. The baseline geometry with a nose radius of 20 mm is sketched in Figure 4.

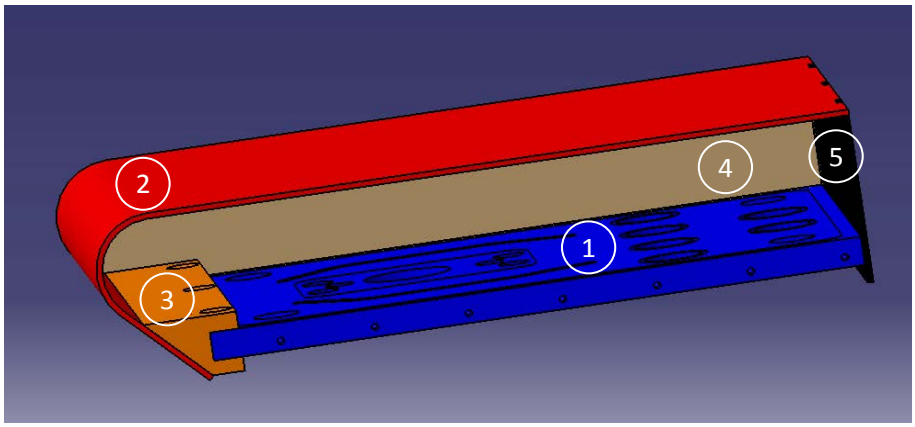

Figure 4: Baseline leading edge geometry for thermal verification tests.

A smaller nose radius of 10 mm was chosen for the second option. This optional geometry was additionally considered for the two passive cooling concepts 1a and 1b. Except for the nose radius, the principal setup is identical for the two geometries. The external CMC skin of the TPS structure (2) is forming the leading edge. Using a copper connector (3) as well as CMC side (4) and rear walls (5) the assembly is mounted on a water-cooled base plate (1).

The test configurations for the individual concepts are based on the two leading edge geometries, but differ in the internal setup in between the CMC skin and the base plate, as shown by the sketches in Figure 5. For the reference concept 0 and for concept 1a the interior is completely filled by a block of insulation material. The two configurations differ only in the material of the CMC skin, which is conventional C/C-SiC for concept 0 and C/C-SiC-HC with integrated highly conductive fibres for concept 1a.

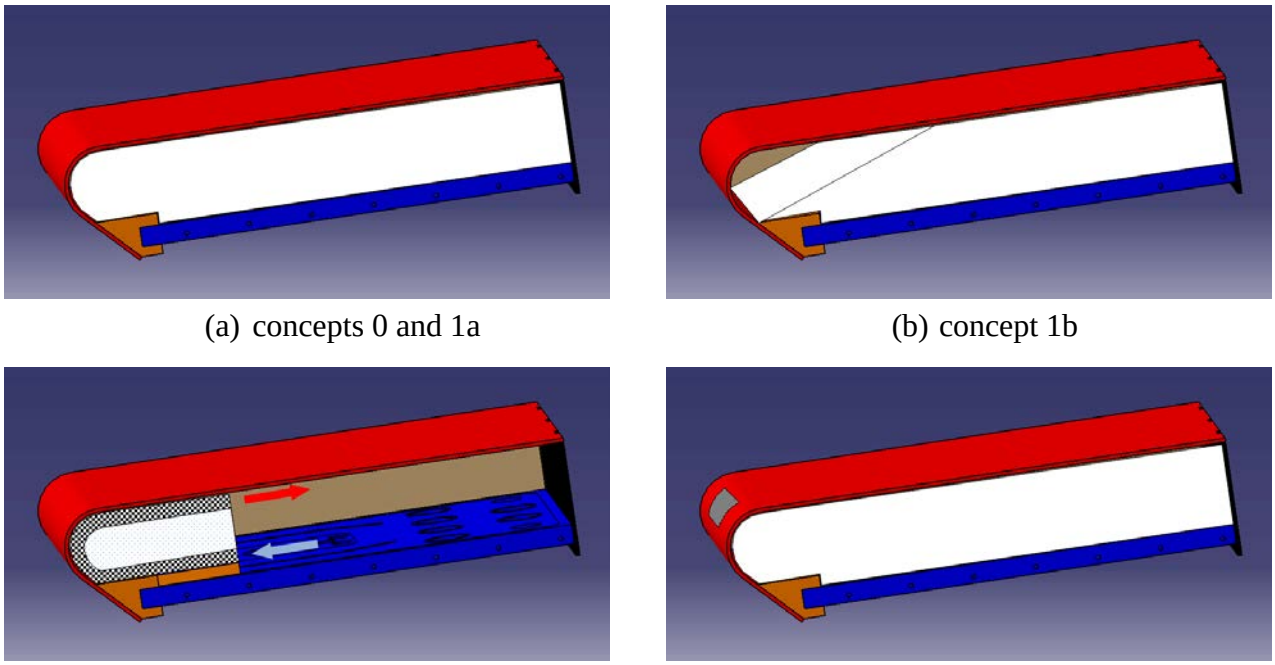

(a) concepts 0 and 1a (b) concept 1b

(c) concept 2a (d) concept 2b

Figure 5: Test configurations for thermal verification

For concept 1b, internal radiation is enabled by removing the insulation block either partially or completely. Conventional C/C-SiC is used for the CMC skin. In a fully passive version, the insulation is being removed in the front part of the leading edge only as sketched in the figure. This configuration allows radiative heat exchange for thermal equilibration in the nose region.

Concept 2a is aiming for active convective cooling of the CMC skin from the backside. This is achieved by integration of a ceramic Si-SiC lattice as a central part of a sandwich which the coolant can be passed through. A block of insulation material is used to form a channel. As shown in Figure 5c, the lattice is covering the backside of the external CMC skin in the nose region. In the non-curved part it is fixed to the internal surface of the CMC skin. The figure does not show required components for coolant storage and distribution.

The second active cooling concept, i.e. concept 2b, is aiming at the transpiration of a coolant through the CMC skin, in order to locally decrease the surface temperature. The coolant is penetrating a porous segment that is integrated into the TPS structure. As sketched in Figure 5d, an insert made of

porous C/C is incorporated into the curved area of the CMC skin in order to provide a permeable passage for gaseous coolants. The system requires a coolant supply system with a coolant reservoir attached to the porous segment.

Appropriate test conditions and test parameters for thermal verification were identified in a numerical study. In addition to the nose radius defined by the leading edge geometry, the total enthalpy of the flow and the angle of attack were considered as main test parameters. Selection was done from a set of four L3K standard test conditions with enthalpy between 9.0 and 11.7 MJ/kg [3]. Baseline test parameters are listed in Table 2 together with preferable second options.

Table 2: Test parameters for thermal verification tests in L3K

Test parameter	Baseline	2nd option
nose radius [mm]	20	10
angle of attack	10°	20°
test condition	THOR-2 (11.0 MJ/kg)	THOR-1 (11.7 MJ/kg)

Numerical simulation also provided support for checking the assumption that the heating of the two generic leading edge geometries in the arc-heated facility L3K can be considered two-dimensional. In this context, 2D and 3D computations of the flow field around the leading edge model were carried out. For simplification, a radiative equilibrium boundary condition was set on the model's surface. Some results are plotted in Figure 6. Figure 6a is showing some temperature isolines on the model surface. Starting at the symmetry plane on the left, the isolines are running in lateral direction mainly. Deviations from this trend are observed in close vicinity to the model's side edge only, indicating a mainly two-dimensional character. This hypothesis is confirmed by Figure 6b where surface temperature distributions in several cutting planes are plotted and compared with the results of a 2D simulation. Except for the cut at y = 0.09 m, i.e. in 7 mm distance to the sidewall, all curves appear coincident with the 2D result [4].

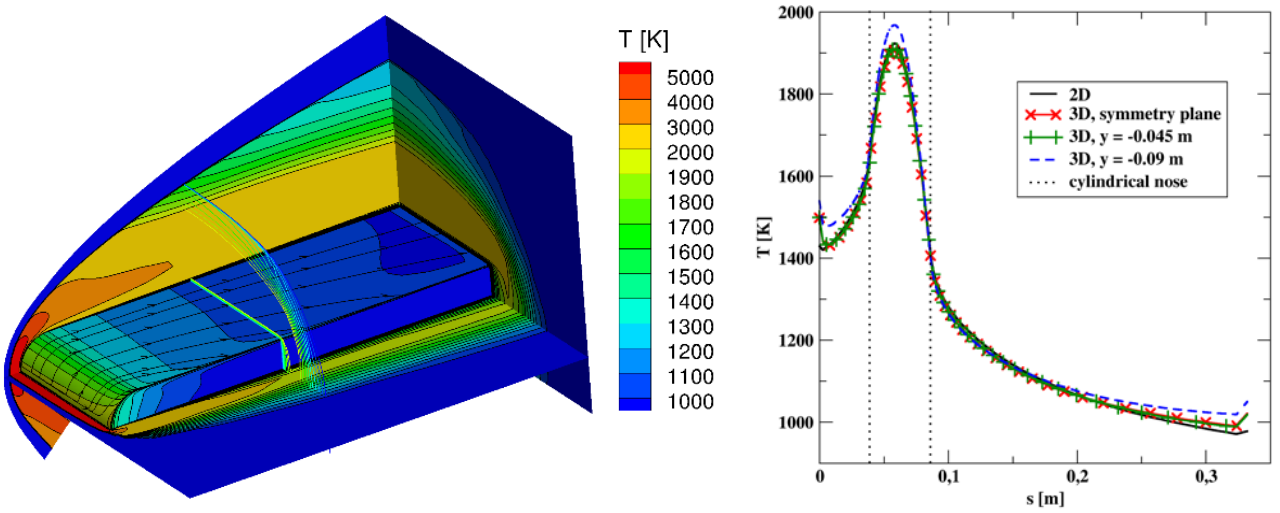

(a) 3D view of temperature isolines and streamlines (b) Surface temperatures distributions

Figure 6: Numerical results of 3D and 2D flow simulations for the baseline geometry

Furthermore, the simulation results showed that surface heat fluxes are insensitive to thermal non-equilibrium effects in the flow field.

For concept 2a, detailed simulations of the flow inside the CMC sandwich structure were carried out to identify the optimal flowpath for the coolant and to check the performance of this concept [5]. Radiative equilibrium conditions were used for the thermal load on the external surface. For the baseline test configuration, the three different flowpaths shown in Figure 7 were considered. The results were compared with regard to the overall temperature level, the lateral homogeneity of the surface temperatures, and the prevention of a recirculation zone within the lattice. Best results were obtained for flowpath configuration 3 where the coolant is following the contour of the leading edge, with an inlet at the bottom and outlet at the top surface.

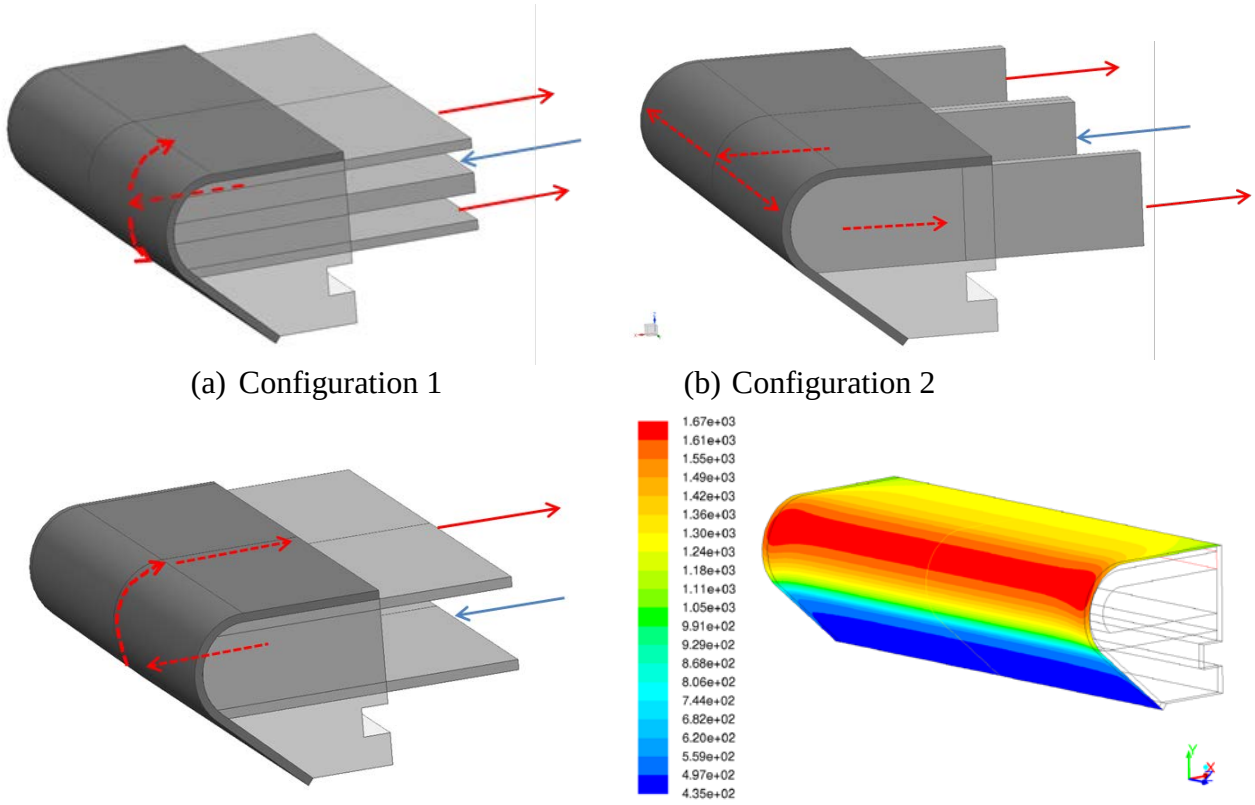

(a) Configuration 1 (b) Configuration 2

(c) Configuration 3 (d) Steady-state temperature contours for configuration 3

Figure 7: Considered coolant flow paths for concept 2a and optimal surface temperature distribution.

As a preparation for coupled simulations for this concept, an aerothermodynamic database (ATDB) was compiled for the L3K test conditions [6]. CFD simulations were conducted for both, the baseline and the optional geometry at angles of attack of 0°, 10° and 20°. Four flow conditions were considered to include enthalpy effects. The ATDB includes radiative equilibrium surface temperatures as well as heat fluxes at a non-catalytic and fully catalytic wall. A large sensitivity to the angle of attack was observed in the flat part of the geometry, while stagnation point heat fluxes came out similar for all angles of attack.

As an exemplary result the radiative equilibrium surface heat fluxes are illustrated in Figure 8 for the baseline test condition THOR-2. Due to high amount of dissociated oxygen in the free stream catalysis has significant influence on the heat flux.

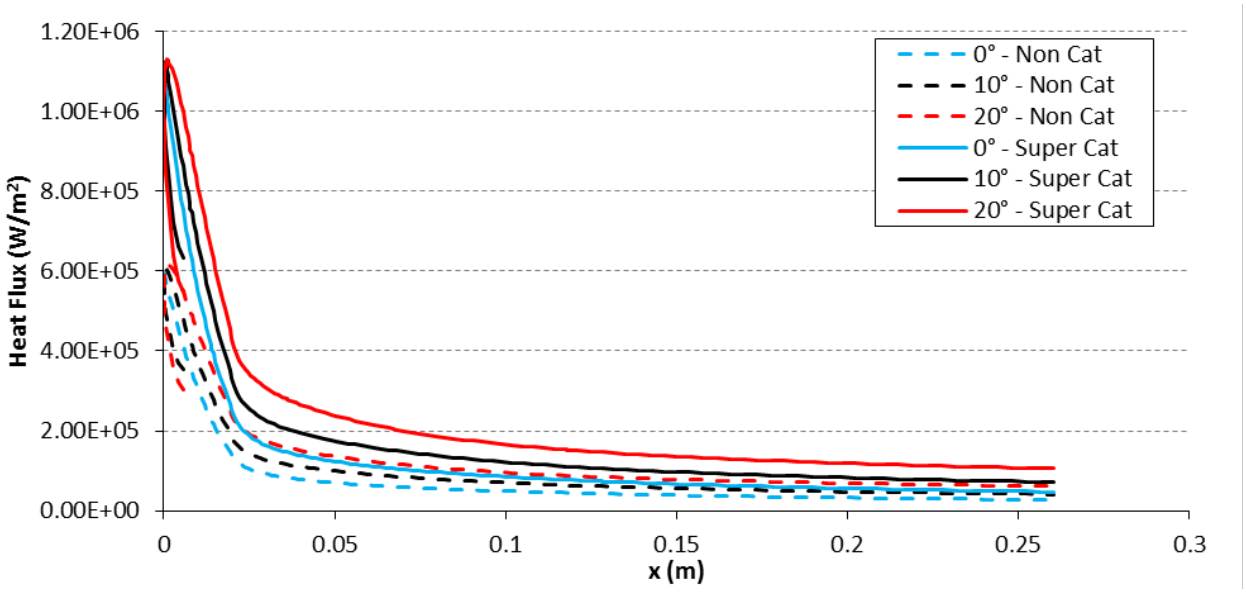

Figure 8: Radiative equilibrium surface heat flux at angle of attack for THOR-2 flow condition.

Manufacturing and Integration

Manufacturing of the ceramic materials and structures as well as their integration into the test assemblies were associated with several challenges. For the external ceramic skin, SiC/SiC was found best-suited for concept 2a and C/C-SiC for all other concepts.

For concept 1a, new processing routes had to be found for the production of large parts of C/C-SiC-HC, i.e. the variant of C/C-SiC with integrated highly conductive fibres. Basically, it turned out that completely new procedure had to be established. First processing trials were performed with flat plates checking the suitability of several fibres with thermal conductivities between 220 and 600 W/mK. The trials were accompanied by mechanical characterization to identify optimal material processing routes. Best homogeneity of the composite was obtained with Mitsubishi fibers with a thermal conductivity of 220 W/mK. Based on these results, Mitsubishi fibers were selected for the leading edge test configuration.

Special moulding tools as shown in Figure 9a were designed to allow for manufacturing the two leading edge geometries within a single production process. Ready prepared leading edges made of C/C-SiC with conventional and highly conductive fibres are shown in Figure 9b and Figure 9c, resp.

For concept 2a, a leading edge made of SiC/SiC was selected in order to achieve a comparable thermal expansion to the ceramic SiC-based lattice that was going to be joined to the leading edge. Instead of an irregular foam, a more regular hexagonal lattice was actually selected according to its better joining capabilities in combination with improved fluid dynamical and mechanical properties. The lattices were manufactured by applying a newly developed replica technique starting from 3D-printed polymeric templates. Some processing steps are illustrated by the photographs in Figure 10. Lattice integration into the leading edge could considerably be improved by applying a slight distortion to the hexagonal cells in order to let them follow the curved contour of the nose part.

(a) Moulding tools

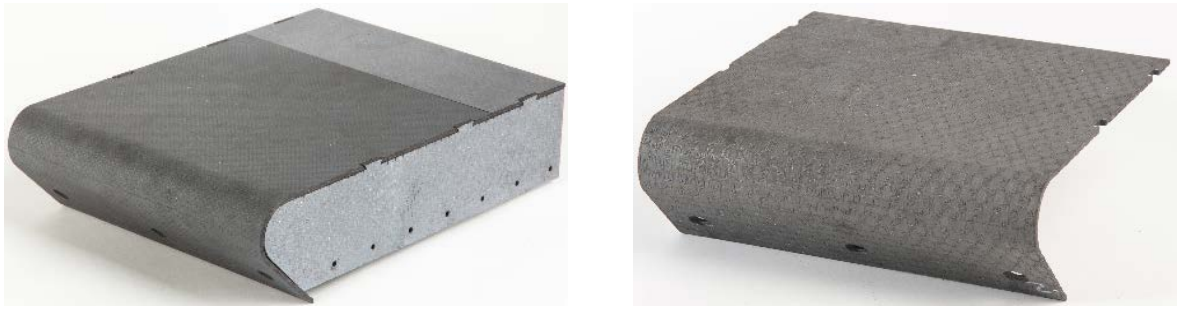

(b) C/C-SiC leading edge for concept 1b (c) C/C-SiC-HC leading edge for concept 1a

Figure 9: C/C-SiC leading edges: manufacturing tools and hardware

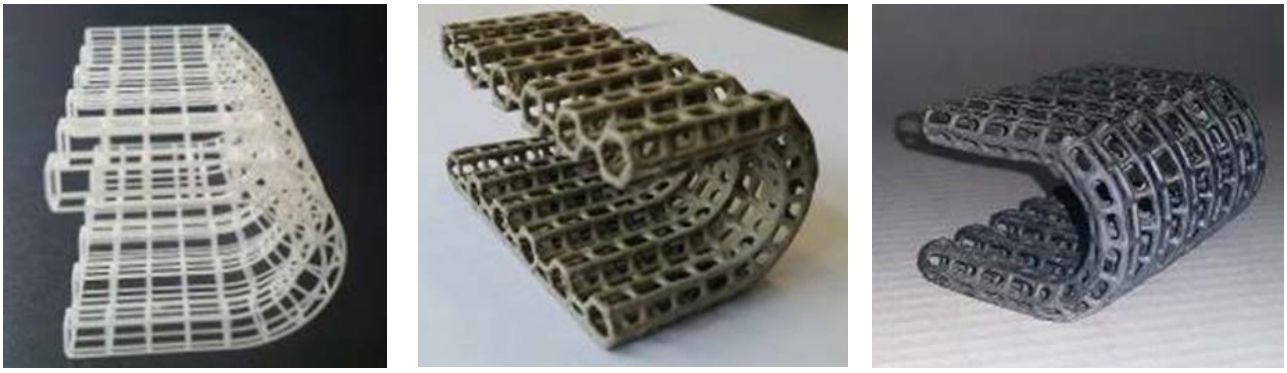

(a) 3D-printed polymeric template (b) Slurry impregnated template (c) Si-SiC lattice component after LSI

Figure 10: Manufacturing of ceramic lattices.

Appropriate joining techniques had to be identified for joining the lattices to the SiC/SiC skin. Several techniques had been identified to be potentially suited for joining a SiC/SiC leading edge to a SiC lattice structure:

- Ceramic adhesives
- Polysilazane modified by different fillers (pre-ceramic polymers)
- Phenolic resin modified by fillers (reaction bonding)

First joining trials were carried out with subsequent analysis of the microstructure and the mechanical properties by microstructural inspection and reaction inspection by chemical analysis. Samples prepared with phenolic resin showed good joints with lowest number of cracks. The results in Figure 11 indicate a good wettability with the phenolic slurry, but also sSome small defects at the interface.

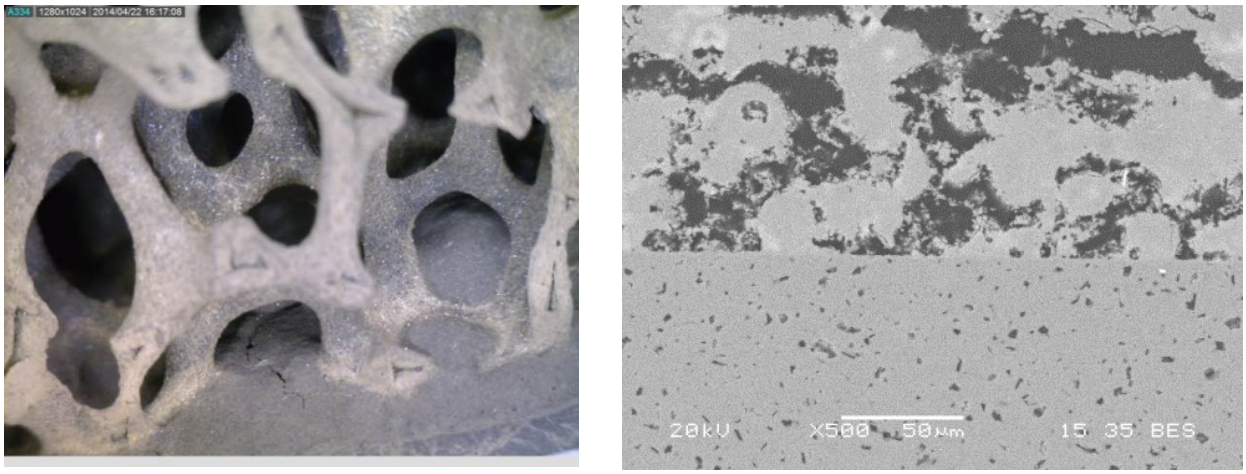

Figure 11: Results of microstructural inspection.

For final selection, a special test setup was elaborated for testing the bonding properties under shear load at the joining interface between the SiC/SiC material and lattices under mechanical loading at high temperatures. Samples and test setup are illustrated in Figure 12.

(a) Samples (b) Setup

Figure 12: Test samples for shear strength measurement

Ceramic adhesives showed reduced adhesion with the base materials at RT. The ceramic adhesive already failed at 830 ºC. Pre-ceramic polymers based on phenolic and polysiloxane modified with filler showed promising results:

- Polysiloxane: shows 425 +/-72 N at 1220 °C
- Phenolic resin: shows 633 +/-153 N at 1220 °C.

Based on the test results, both bonding systems were found suitable for application, since they showed residual strength up to 1520°C, which is a substantial thermal safety margin [7]. Eventually, the leading edge test hardware shown in Figure 13 was prepared with phenolic resin due to its better strength at high temperatures of 1220°C.

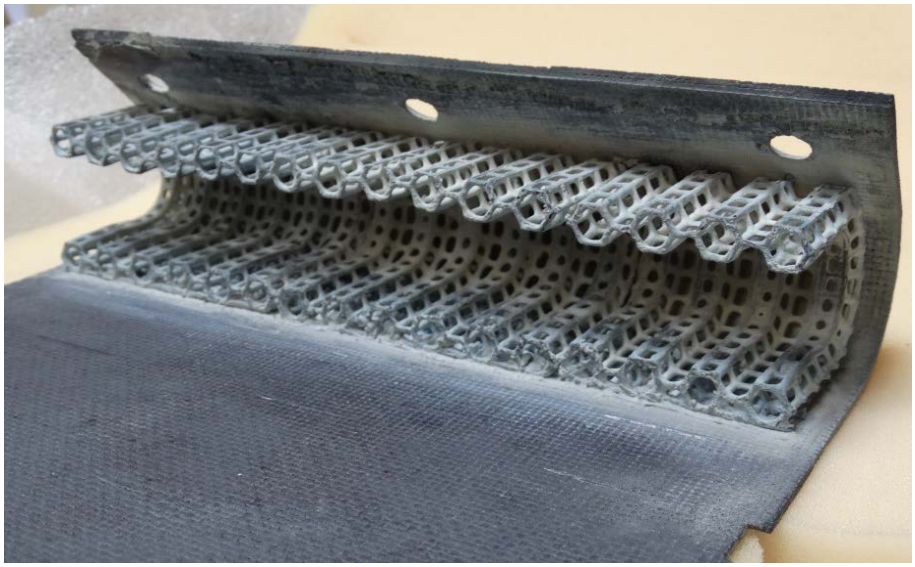

Figure 13: SiC/SiC leading with joined lattices.

In the context of concept 2b, porous C/C-based structures had been identified well-suited for the experimental verification of transpiration cooling. With a newly developed integration technique based on electroplating the porous structures could be embedded leak-free into a metallic frame which also served as coolant reservoir. Thus, the whole coolant supply system could be kept small-sized, which is a key requirement for local application of transpiration cooling in a leading edge environment. Porous substructures were prepared for test campaigns in DLR's arc-heated facility L3K (Figure 14a) and JAXA's shock tunnel facility HIEST (Figure 14b).

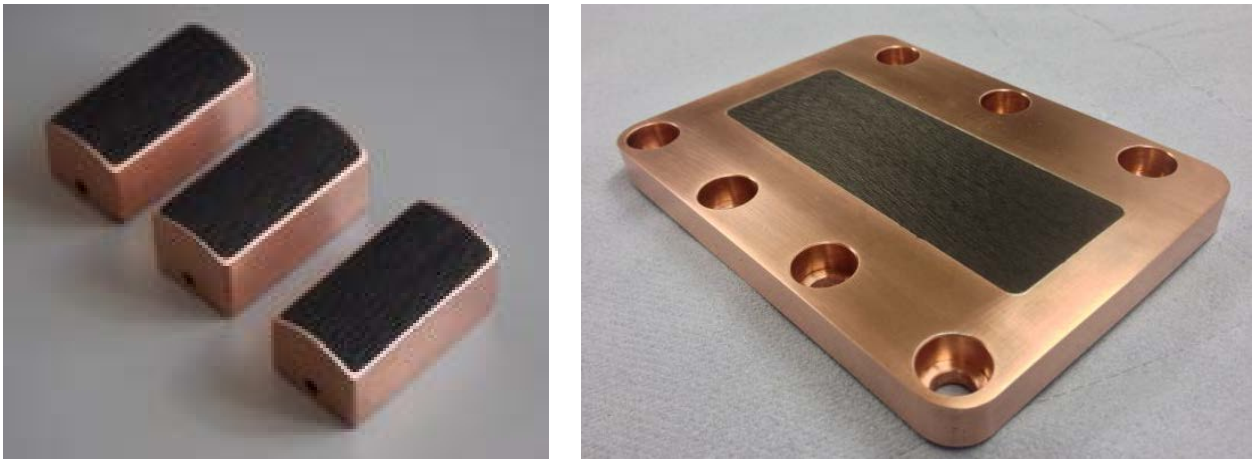

(a) for leading edge assembly (L3K) (b) for flat plate assembly (HIEST)

Figure 14: Electroplated porous substructures.

Experimental Verification

Thermal verification tests were carried out in the arc-heated facility L3K using the leading edge assemblies. For all considered concepts, the test assemblies were exposed to identical high enthalpy test conditions. Photographs of the interior of the final test assemblies are shown in Figure 15. A test assembly mounted in the L3K test chamber is shown in Figure 16.

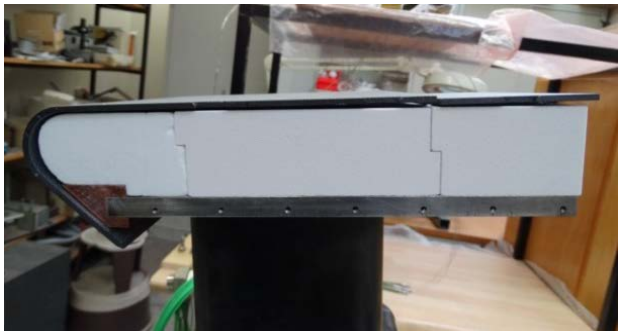

(a) concepts 0 and 1a

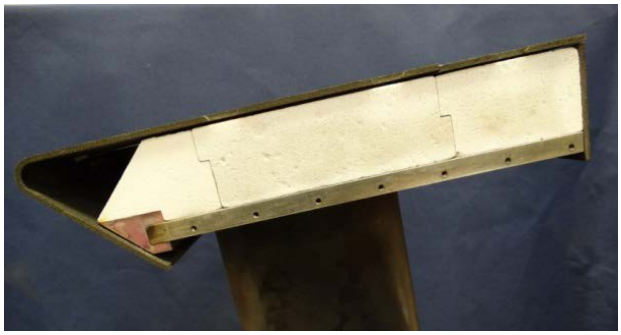

(b) concept 1b

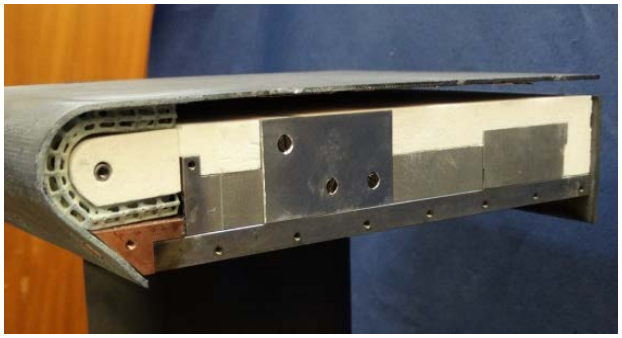

(c) concept 2a

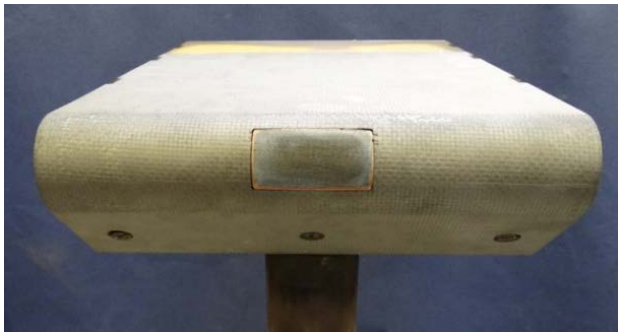

(d) concept 2b

Figure 15: Leading edge test assemblies

The tests were carried out as transient tests to steady-state conditions. In comparison to the reference concept, the final temperature readings were used to assess the thermal performance with particular consideration of the two principal targets of THOR, i.e.

- thermal equilibration and
- reduction of the stagnation temperature.

Temperature measurements were carried out with thermocouples on the inner surface of the CMC skin. Surface temperatures were measured with an infrared camera system and with pyrometers [8]. A typical infrared image is shown in Figure 16.

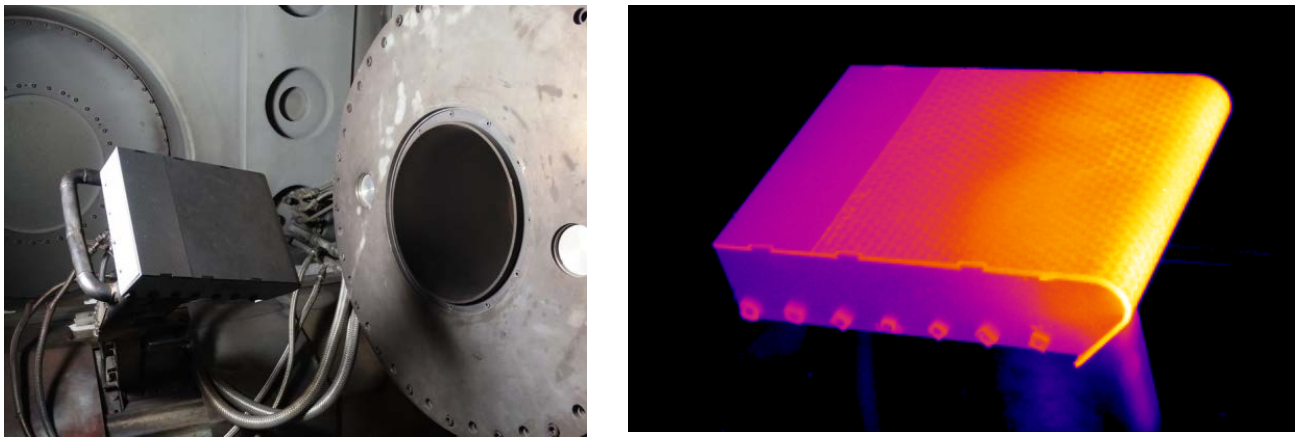

Figure 16: Test assembly mounted in L3K (left) and typical infrared image (right)

Passive cooling concepts 1a and 1b

The thermal verification tests related to the two passive cooling concepts 1a and 1b were carried out in combination with the tests on the reference concept 0. Concept 0 and 1b could be set up with the same external CMC skin, made of conventional C/C-SiC. Only the model's internal configuration had to be changed for concept 1b by opening a cavity at the nose. For the verification of concept 1a, the C/C-SiC skin was replaced by a leading edge made of C/C SiC-HC with integrated highly conductive fibres. For the intrinsic concept 1a, the internal configuration was kept fully insulated, identical to the reference concept 0. With a change of the internal configuration as for concept 1b, a combined application of concepts 1a and 1b could be realized additionally.

Thermal equilibration was observed for both passive concepts, i.e. 1a and 1b. In particular, the opening of a small cavity at the nose with concept 1b resulted in a significant settlement of temperatures differences. The plot in Figure 17a provides a comparison of the final thermocouple readings on the internal surface of the CMC skin for concepts 1b and 0. The location of the cavity is marked by red background colour. At the stagnation point (x=-20 mm) the temperature reading is reduced by nearly 100 K after opening the cavity. At the downstream end of the cavity the temperature is increased by almost the same amount according to the radiative heat exchange. No major differences are observed further downstream, where insulation is installed in both cases.

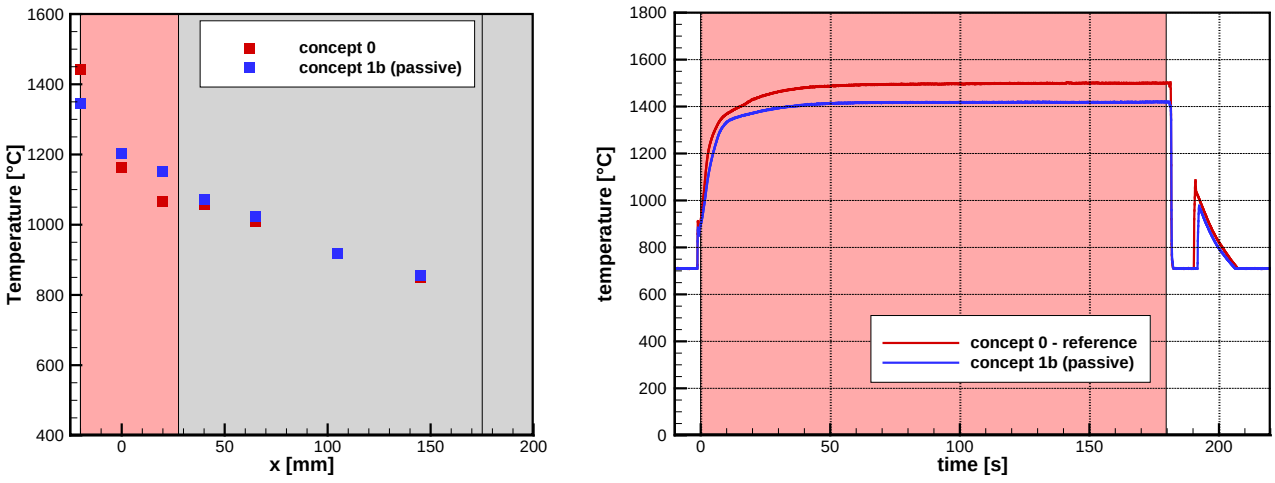

(a) thermal equilibration (b) reduction of stagnation temperature

Figure 17: Thermal performance of concept 1b.

The reduction of the stagnation temperature is the most important demand for improvements to thermal management of a reusable ceramic TPS structure. With 70 K and 80 K, resp., comparable temperature reductions were measured for the two passive concepts 1a and 1b. For concept 1b, the surface temperature readings at the stagnation point are compared with the reference measurement in Figure 17b.

By combining concepts 1a and 1b, the temperature reduction could be enhanced to more than 100 K. At first glance, these differences appear small, but according to the strong temperature dependence in the Stefan-Boltzmann law, the correlated differences in radiative heat fluxes are significant. Considering that the heat load can be increased according to the forth power of the temperature ratio, a substantial heat load Δq can be applied additionally to reach the stagnation temperature of the reference configuration [9]. Corresponding data are listed in Table 3. An increase of 14% appears possible for concept 1a, for concept 1b the percentage increases to 17%, and for the combined application of both concepts the heat load might be increased by 21%. Lower values were evaluated for the smaller leading edge radius.

Table 3: Cooling efficiencies for passive cooling concepts

Geometry	**Concept**	**ΔT_{max}**	**$\Delta q/q_{max,ref}$**
		[K]	
Baseline (R = 20 mm)	1a	70	0.14
	1b	80	0.17
	1a + 1b	103	0.21
Optional (R = 10 mm)	1a	45	0.10
	1b	36	0.08

Coupled numerical simulations were carried out for numerical rebuilding of the experiments on the passive cooling concepts. For both, the baseline and optional geometry, the four configurations shown in Figure 19 were considered numerically [10].

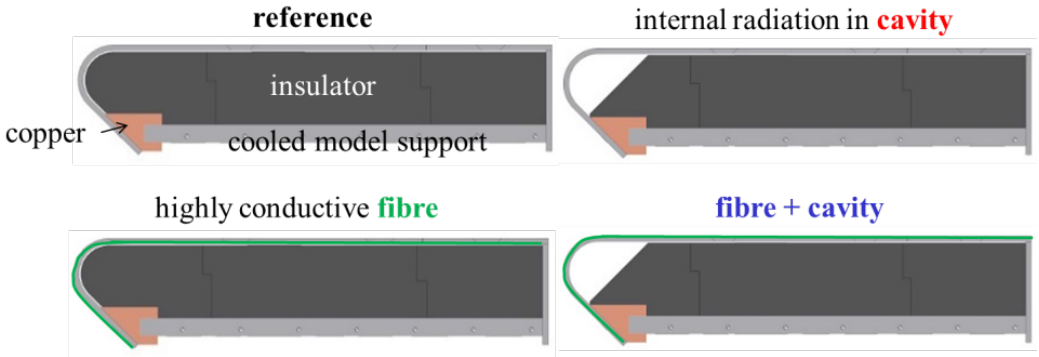

Figure 18: Sketch of considered configurations.

A loose coupling strategy was applied for the simulations. In a first step, surface heat fluxes were determined from flow field simulations assuming radiative equilibrium on the surface. Based on these loads, a structural simulation was carried out, providing improved surface temperature data for the flow solver. The workflow for structural simulations is illustrated in Figure 20. Generally, only a few iterations were required to reach convergence.

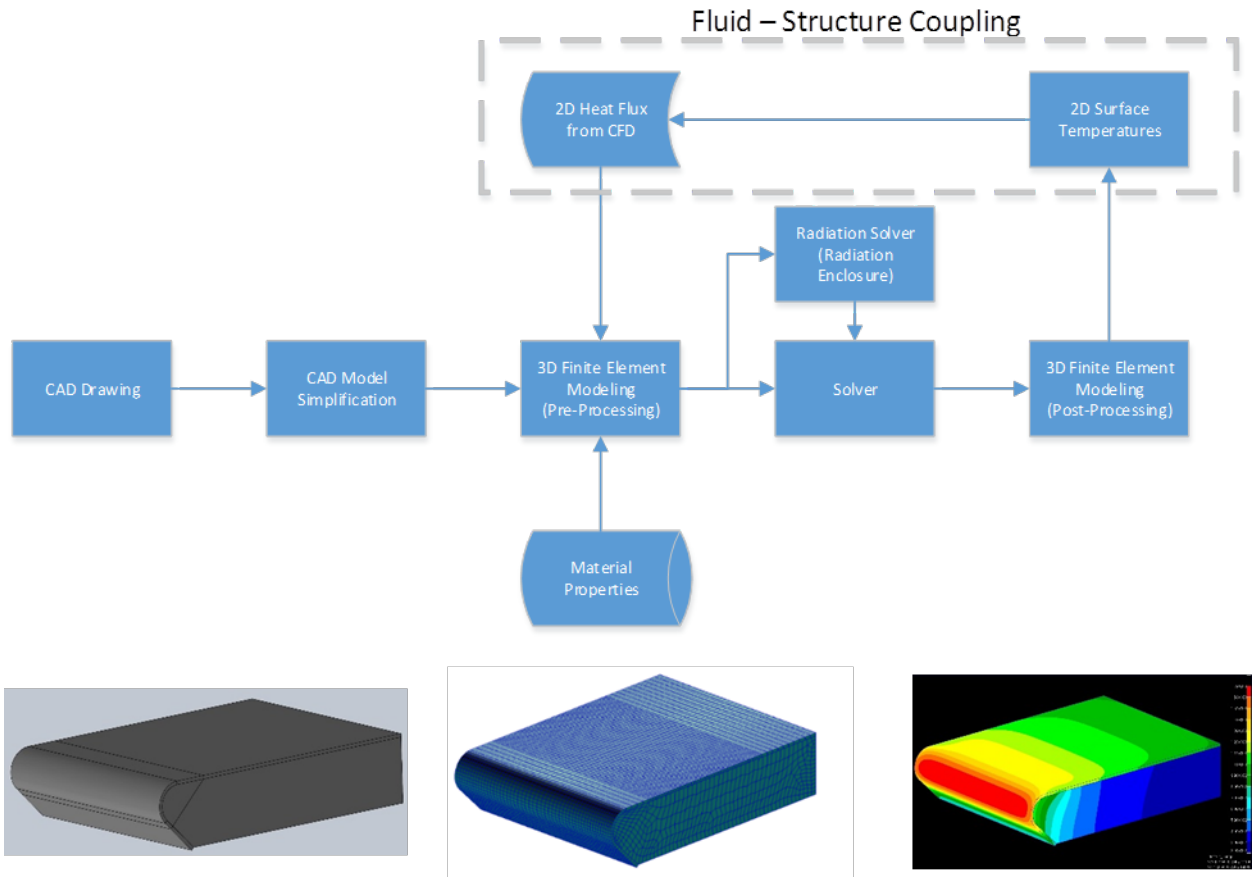

Figure 19: Workflow of structural simulations .

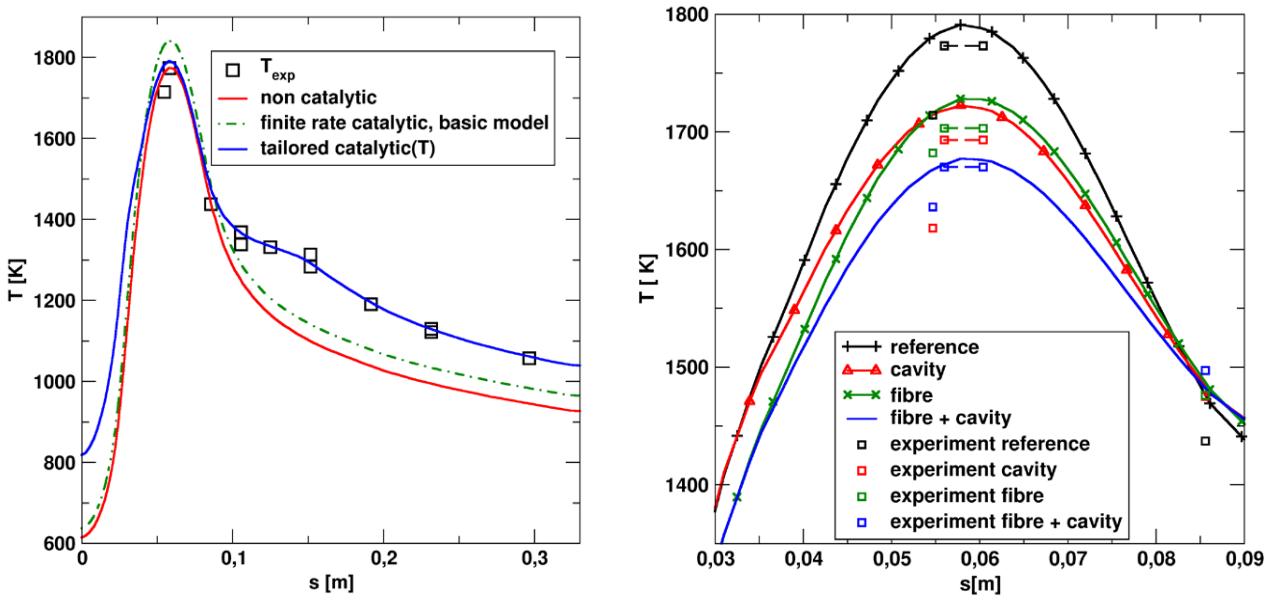

(a) Surface temperature for various catalysis models

(b) Temperature profiles at the leading edge

Figure 20: Comparison of computed temperature profiles with measured data.

Various models were applied to account for the surface catalycity in numerical rebuilding. When comparing with the experimental results, differences in the catalytic behaviour along the model surface were observed. In the nose part catalytic effects were almost negligible, while the flat part of the surface appeared highly catalytic. To account for these differences a tailored catalysis model was defined [4] based on the experimental results on the reference concept 0 (see Figure 21a), and applied afterwards to the other concepts. The reduction of stagnation temperatures could be confirmed with the tailored catalysis as the plot in Figure 21b demonstrates.

Concept 2a: CMC-Sandwich

Concept 2a was associated with the most complex test configuration. Actually, two test configurations were prepared for thermal verification. The first one was the above mentioned SiC/SiC leading edge with the lattices joined (see Figure 13), the second setup was based on a C/C-SiC leading edge. For the latter, the lattices were kept unjoined in order to avoid problems related to CTE mismatch. Eventually, most of tests were carried with the C/C-SiC skin, since the SiC/SiC skin got locally damaged during run-in tests.

Coolant gas and coolant flow rate were varied during the test campaign. In a first subseries with air cooling, the flow rate was gradually increased from 2.5 g/s to 10 g/s. The influence of cooling is illustrated by the plot in Figure 18a, showing temperature profiles extracted from infrared images along a representative line in streamwise direction. The curved part of the leading edge is marked by a red background, the grey background indicates the part of the flat surface with lattices below. With increasing coolant flow rate, temperatures decrease all along the surface. Largest differences are observed close to the stagnation point and at the downstream end of the lattice on the flat surface. Even at the lowest flow rate of 2.5 g/s temperatures are below the results found for the passively cooled reference configuration.

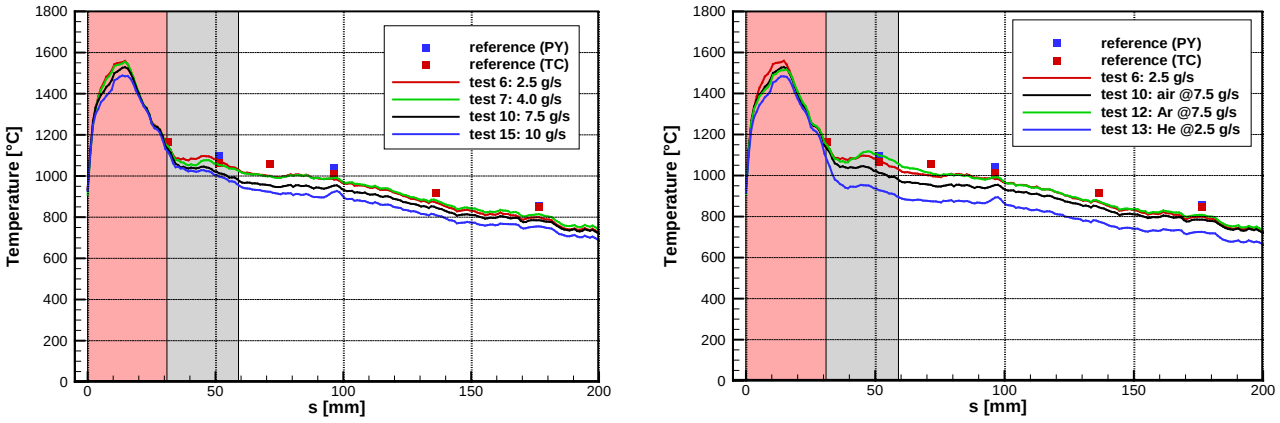

(c) variation of flow rate (air cooling) (d) variation of coolant gas

Figure 21: Surface temperature profiles from thermal tests on concept 2a.

In a second subseries the coolant gas was varied. Air and argon were compared at a flow rate of 7.5 g/s. The temperature distributions in Figure 18b indicate a similar cooling efficiency for both coolants in the stagnation region. Higher temperature reductions, however, were measured, when helium was used as coolant. Due its much higher heat capacity, the measured temperatures are below the results obtained for air and argon, even at a significantly lower flow rate of 2.5 g/s. Correlated cooling efficiencies are listed in Table 4.

Table 4: Cooling efficiencies for concept 2a

Coolant	Flow rate	ΔT_{max}	$\Delta q/q_{max,ref}$
	[g/s]	[K]	
Air	7.5	33	0.08
Air	10	71	0.18
Argon	7.5	39	0.09
Helium	2.5	78	0.20

Concept 2b: Transpiration Cooling

For the transpiration cooling concept 2b, a quantitative evaluation of thermal performance could not be achieved, since steady-state conditions could not be reached in the thermal tests. As illustrated by the series of infrared images in Figure 22, intensive cooling was observed at the porous segment as well as downstream along the model's surface, but the zoomed images indicate increasing temperatures at the stagnation line which sooner or later exceeded the operational limits of the C/C material. Numerical predictions did not include intense stagnation line heating and it could not even be rebuilt with more detailed simulations after the experimental campaign.

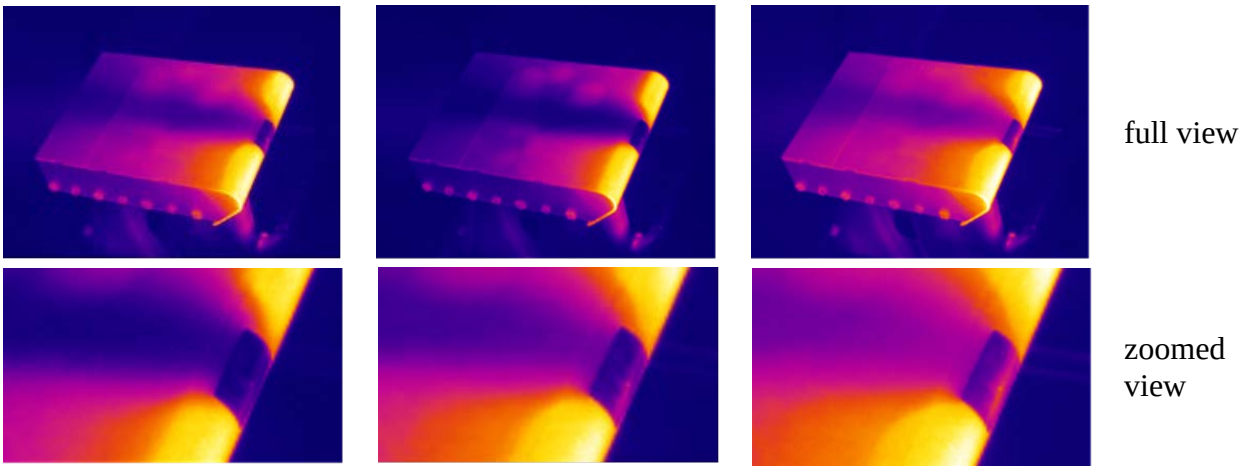

(d) 20 s (e) 40 s (f) 60 s

Figure 22: Sequence of IR images from a test on concept 2b.

In addition to thermal tests, transpiration cooling was also subject of a test campaign in JAXA's shock tunnel HIEST, in order to investigate the interference of the emanating coolant gas with the boundary layer. The tests were carried out on the flat plate test assembly shown in Figure 23. A porous injector that was installed in a short distance to the leading edge allowed for coolant supply at various flow rates. Five tests conditions were considered with a variation of Reynolds number and total enthalpy [11]. Helium and nitrogen were used as coolants. Pressure and temperature measurements in the wake of the porous segment allowed for checking the boundary status. Evaluation of the test results was done in comparison to reference tests performed without cooling.

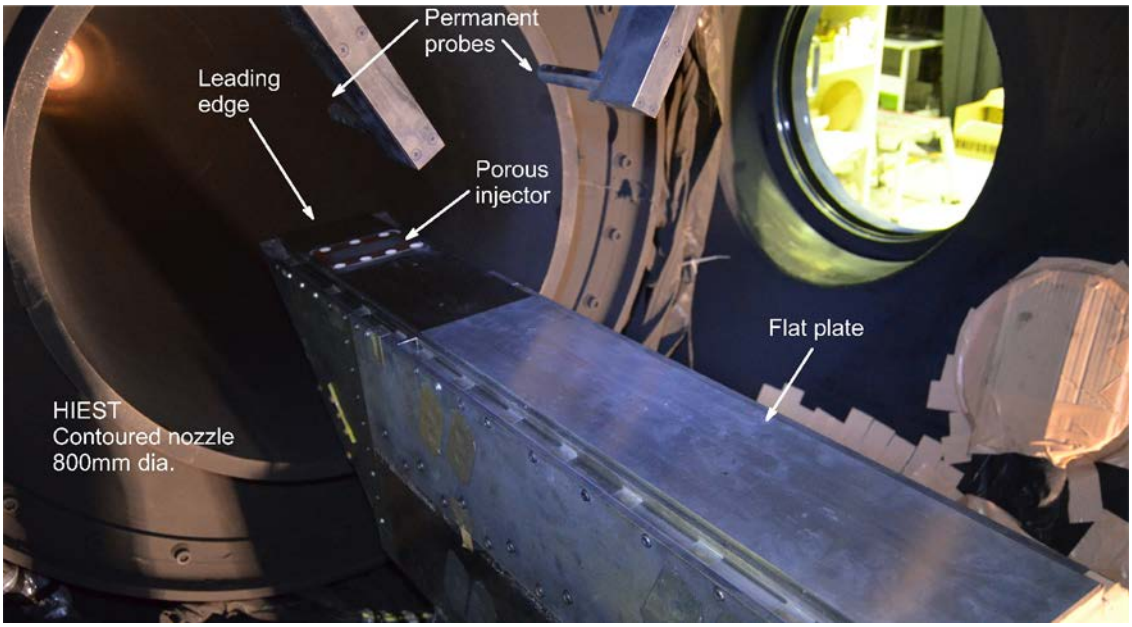

Figure 23: Test setup for transpiration cooling tests in the HIEST shock tunnel.

Transpiration cooling, in particular the interference of the emanating gas with the boundary layer, was investigated in the test campaign in the HIEST shock tunnel. Five tests conditions were considered with a variation of Reynolds number and total enthalpy. Helium and nitrogen were used as coolants. As illustrated by the plots in Figure 24 cooling was found more effective for a laminar boundary layer, i.e. at lower Reynolds numbers. With increasing coolant flow rate, however, the risk of boundary layer transition was enhanced. A slight decrease of cooling efficiency was observed at highest enthalpy [12].

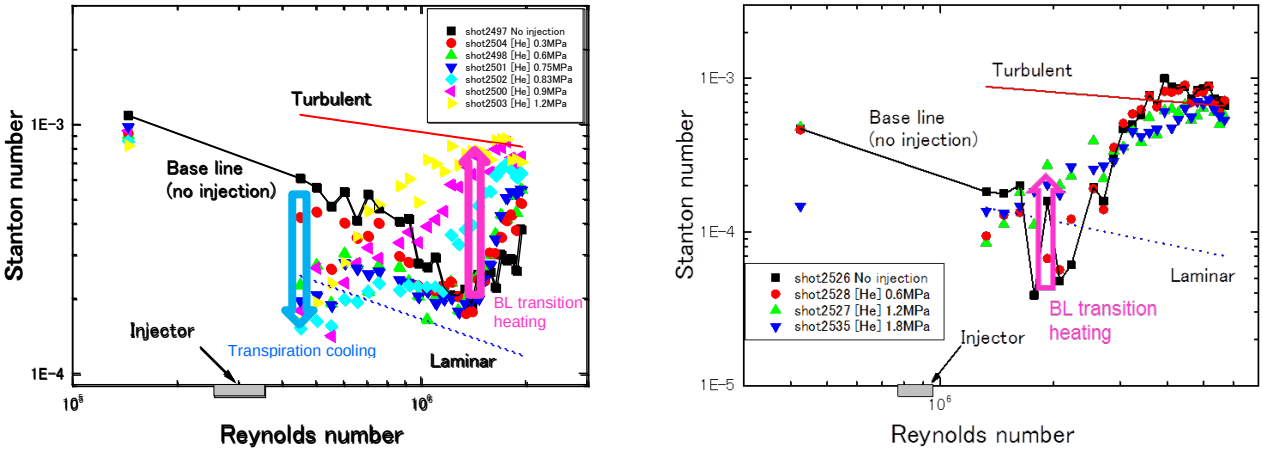

(a) Condition 3 (low Re number) (b) Condition 2 (high Re number)

Figure 24: Heat flux distribution on the flat plate with Helium cooling.

The experimental could principally be rebuilt by numerical simulations. As an example, Figure 25 provides a comparison for conditions 3 with nitrogen cooling [6]. The numerical results slightly overpredict the effectiveness of the laminar cooling in the wake of the porous segment. The turbulent simulations show a good agreement with the fully turbulent conditions with the experimental results

close to the downstream end of the flat plate. The simulations also confirm that there is a negligible reduction in the heat flux with increased blowing rate in the turbulent region.

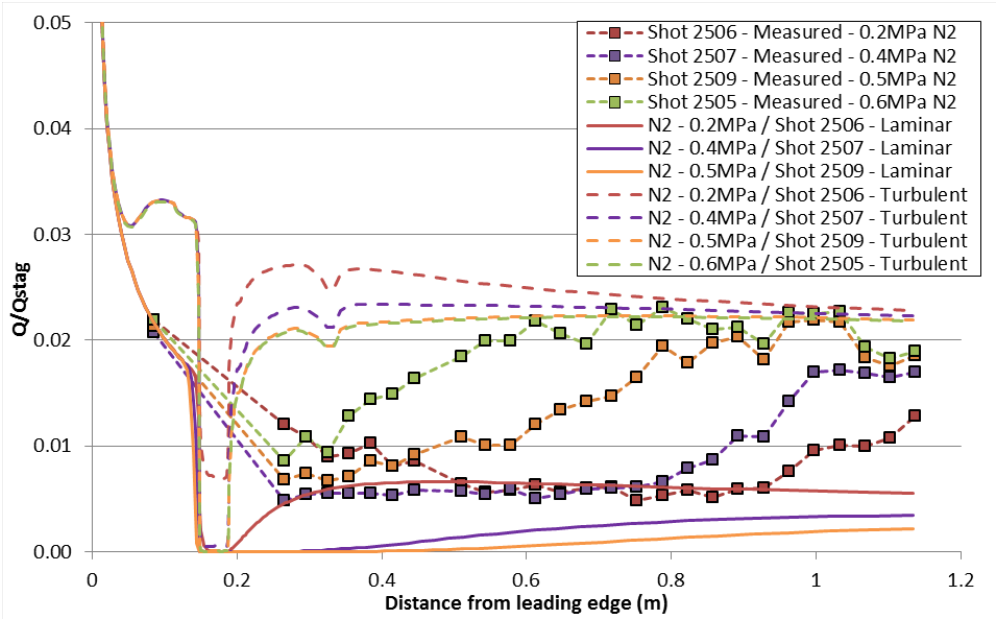

Figure 25: Comparison of numerical and experimental data for condition 3 with nitrogen cooling.

Extrapolation to Flight

A central element of the activity's final synthesis was related to extrapolation to flight. Two reference configurations were considered (see Figure 26), i.e.

- a winged variant of IXV evolution as a representative for an atmospheric entry vehicle, and
- the SpaceLiner as a hypersonic transport vehicle.

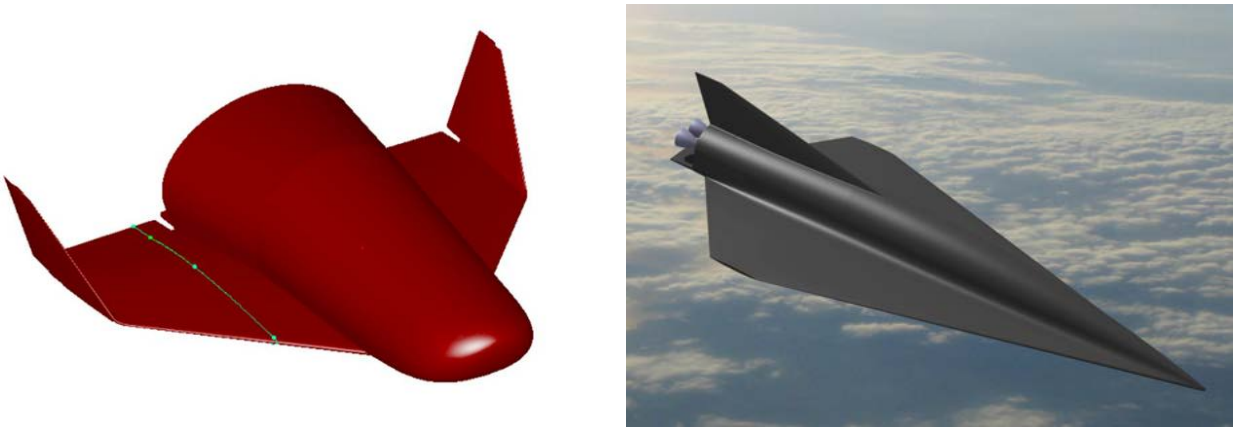

(a) IXV evolution (re-entry) (b) SpaceLiner (hypersonic transport)

Figure 26: Reference vehicles considered for extrapolation to flight

Numerical simulations were performed for both vehicles' wing geometries at a realistic flight conditions using the structural models to calculate the thermal response and thus effectiveness of the four considered cooling concepts. For the IXV evolution wing, only a moderate reduction of the peak temperature was determined for concept 1a. With the cavity, however, defined as shown in Figure

27a, radiative heat exchange according to concept 1b was found more effective by a factor of 2.5 [13]. As for the L3K test configuration, the most effective temperature reduction was determined for the combination of the two passive techniques, which caused a reduction of 190K in the peak temperature. Correlated temperature profiles are illustrated in Figure 27a. Much higher temperature reduction can be obtained with transpiration cooling, even when considering the limits for avoiding boundary layer transition. For the active cooling, however, the complexity of integrating the cooling system and design optimization to minimize the cost of additional weight due to coolant must be considered additionally [14].

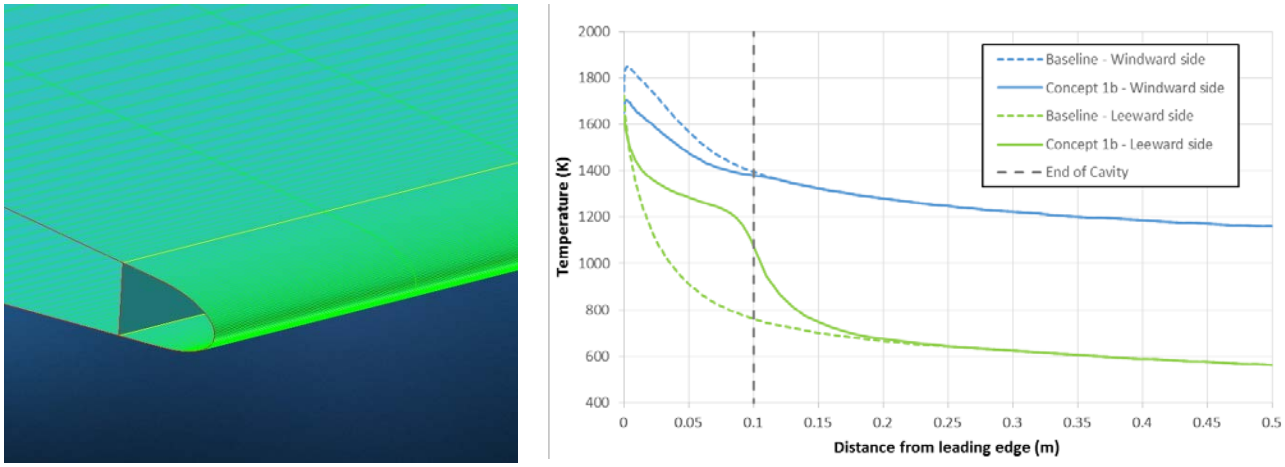

(a) Leading edge with cavity (b) Computed temperature profiles

Figure 27: Influence of a cavity on the heating of the IXV evolution wing

Conclusive Remarks

Improvements to thermal management capabilities could be verified for all four considered concepts. During the experimental campaign in L3K considerable reductions of stagnation temperatures were evaluated for the leading edge test configurations. These reductions are correlated with a considerable potential to increase the applicable heat loads. The experimental results confirm a TRL level of 2-3 for each concept.

In addition, there are indications that the evaluated improvements might be further increased. For concept 1a, further improvements appear possible, since there are still fibers available with a higher thermal conductivity. Those might be integrated, if appropriate processing routes can be found in order to manufacture homogeneous composite materials.

Considerable temperature reductions in combination with a significant thermal equilibration were found for the test configuration with concept 1b. Here, the geometry of the radiation cavity was chosen almost arbitrarily. Thus, geometric optimization seems promising. This expectation is supported by the fact, that numerical simulations on flight configurations provided even higher improvements than evaluated for the test configuration.

For the active cooling concept 2a, the experimental results showed a general temperature reduction for the most effective cooling conditions. Accordingly, a considerable fraction of the coolant's potential for heat exchange could not be utilized in the highly loaded areas, but was transferred further downstream. Thus, there should be technical possibilities to improve e.g. the lattices in the coolant channel with respect to a more intense heat exchange with the external skin.

Qualitatively, transpiration cooling showed highest potential for the reduction of maximal temperature. In the test configuration, however, the integration was found not optimal, but improved solutions are already under development and might be ready for use soon.

With regard to the concepts and technologies considered in THOR, a perspective for further development and use was prepared as a use plan from an industrial point of view [15]. For the cooling concepts the use plan starts from a TRL of 2-3 which could successfully be demonstrated within the project. In addition, the use plan includes several sub-technologies which were initiated or further development within THOR and are applicable also to non-space markets. Some of those already reached a TRL of 5.

References

[1] J. Barcena, B. Esser, M. Kuhn, *Guidelines for the selection of the reference configurations*, THOR deliverable D2.2

[2] I. Petkov, *Report On Thermal Management for CMC Structures*, THOR deliverable D3.2

[3] B. Esser, *Report on Innovative Thermal Management Concepts*, THOR deliverable D3.1

[4] V. Hannemann, *Report on Simulations with Thermal Fluid-Structure Interaction*, THOR deliverable D4.5

[5] L. Ferrari, A. Ortona, M. Barbato, *Report on CFD through the foam simulations*, THOR deliverable D4.3

[6] J. Caldwell, L. Haynes, G. Parnaby, *Report of flow simulations for wind tunnel conditions*, THOR deliverable D4.1

[7] I. Petkov, M. Portaluppi, V. Liedtke, *Report on Material Characterization*, THOR deliverable D6.1

[8] B. Esser, *Experimental Setup for Validation Tests in Arc-Heated Facilities*, THOR deliverable D6.2

[9] B. Esser, *Validation Tests Results in Arc-Heated Facilities*, THOR deliverable D6.3

[10] A. Okan, S. Ontaç, *Report on Structural Simulations with Intensive Radiative Heat Exchange*, THOR deliverable D4.4

[11] H. Tanno, K. Itoh, *Experimental setup for shock tunnel tests*, THOR deliverable D6.4

[12] H. Tanno, *Validation test results from shock tunnel facility*, THOR deliverable D6.5

[13] J. Caldwell, *Report on Flow Simulations for Flight Condition*s, THOR deliverable D4.2

[14] C. Chiarelli, *Synthesis and Extrapolation to Flight*, THOR deliverable D2.3

[15] M. Portaluppi, *Use plan from the industrial end user and industrial partners*, THOR deliverable D7.2

4.1.4 Project Website and General Contacts

For the THOR project an internet portal has been established. It is accessible under

http://www.thor-space.eu

The web portal includes a public part that is describing the details of the THOR approach, the main objectives, the structure of the project including information on the partners of the consortium..

The THOR project can be contacted via the coordinating partner DLR. Contact points are

a) for technical and scientific matters:
   Dr. Burkard Esser, DLR, Institute of Aerodynamics and Flow Technology, Linder Höhe, 51170 Köln, Germany, Burkard.Esser@dlr.de
b) for administrative, legal and financial matters:
   Uliana Eckler, DLR, Contract administration Köln, Linder Höhe, 51170 Köln, Germany, Uliana.Eckler@dlr.de

Project partners are:

- DLR: Deutsches Zentrum für Luft- und Raumfahrt, Germany
- TECNALIA: Fundacion Tecnalia Research & Innovation, Spain
- TUBITAK: Türkiye Bilimsel ve Teknolojik Arastirma Kurumu, Turkey
- FGE: Fluid Gravity Engineering, United Kingdom
- ERBICOL: Erbicol SA, Switzerland
- SUPSI: Scuola Universitaria Professionale della Svizzera Italiana, Switzerland
- AAC: Aerospace and Advanced Composites GMBH, Austria
- TAS-I: Thales Alenia Space Italia S.p.A., Italy
- JAXA: Japan Aerospace Exploration Agency, Japan